PAPER NO.617

A TWO ZONE MODEL FOR LONGITUDINAL DISPERSION IN CHANNELS WITH IDEALIZED POOLS AND RIFFLES

BY
Dr. Zulfiqar Ali

A Two-Zone Model for Longitudinal Dispersion in Channels with Idealized Pools and Riffles

Zulfiqar Ali[1], Eric M. Valentine[2] and David C. Swailes[3]

Abstract

A one-dimensional, two-zone mathematical model, comprising a pair of advection-dispersion equations coupled by a mass-exchange term, is proposed to study longitudinal dispersion in channels with sequences of pools and riffles. An implicit finite-difference numerical scheme is employed, and its effectiveness is assessed with reference to known analytical solutions. Moreover, sets of longitudinal dispersion experiments were performed on various simple geometries of sequences of pools and riffles developed in a laboratory flume. The results were compared with corresponding numerical solutions to calibrate the two-zone model.

INTRODUCTION

It is widely acknowledged that simple Fickian models do not provide accurate descriptions of the longitudinal transport of contaminants in natural channels, especially during early stages of the mixing process (Young and Wallis, 1993). Even after the initial period defined by Taylor (1954), skewed concentration-time profiles and nonlinear growth of variance of the contaminant clouds have been observed (Day, 1975). Hays (1966) developed a dead-zone model to explain the long tails observed in concentration-time profiles. Subsequently, Thackston and Schnelle (1970), Valentine and Wood (1977, 1979a, 1979b), Bencala and Walters (1983), Chikwendu and Ojiakor (1985) and others developed models to explain mixing processes in natural channels.

In line with earlier works, [see for example Smith (1976, 1979), Bencala and Walters (1983), Chikwendu and Ojiakor (1985), Seo (1990a, 1990b), Seo and Maxwell (1992)] and considering flow characteristics of pools and riffles (Miller and Wenzel, 1984, 1985), a one-dimensional two-zone model consisting of flow and slow zones is proposed. The two-zone model is applied to study longitudinal dispersion in channels with sequences of pools and riffles. This model is a more general form of the dead-zone mechanism having advection and dispersion terms in both zones along with the dead-zone parameters. The advection and dispersion terms of the slow zone simplify the calculation of dead zone parameters with varying discharges. The proposed model could be of value for channels with pools and riffles. Such channel flows are highly turbulent, with large variations in flow velocities and cross-sectional areas (Bencala and Walters, 1983; Bhowmik and Demissie, 1982; Miller and Wenzel, 1985). The near-bed velocity of pools also increases progressively with the increase in flow rate (Sear, 1996).

---

[1] Assistant Professor, Department of Civil Engineering, University of Engineering & Technology Lahore, Pakistan

[2] Senior Lecturer, Department of Civil Engineering, University of Newcastle upon Tyne, UK

[3] Lecturer, Department of Engineering Mathematics, University of Newcastle upon Tyne, UK

As in Fig. 1, the flow is divided into two zones: a flow zone (zone 1) and a boundary slow zone (zone 2). The flow zone is an upper region of water having larger flow velocities compared to the slow zone, which is mainly controlled by surface roughness and pools. This two-zone model was studied numerically using an implicit-finite difference method. The numerical results were assessed with reference to analytical solutions for uniform flows (Chikwendu and Ojiakor, 1985) with a constant dispersion coefficient. Computer programs were developed for the numerical and the analytical solutions of the model. The programs computed concentration variations, displacement, velocity, spatial variance and total mass in the flow and the slow zones.

To create a reliable experimental database and to validate and calibrate the proposed two-zone dispersion model, hydraulic and longitudinal dispersion experiments for a variety of flow rates were performed on four idealized geometries of six pool-riffle sequences constructed in a laboratory flume. Laboratory experiments were also performed to measure mass exchange coefficients between the flow and slow zones.

The aims of this research were:

a) to study longitudinal dispersion and the hydraulics of channels with sequences of pools and riffles.
b) to test and validate the numerical schemes with the analytical solutions, and
c) to calibrate the proposed model parameters with the experimental data.

THE TRANSPORT MODEL AND NUMERICAL METHOD

In this paper, the transport of neutrally buoyant solute material introduced into a fully developed turbulent flow in an open-channel is considered. In particular, attention is given to longitudinal transport in channels that possess bed storage zones (pools) along their length (Fig. 1). Stretches between pools (the riffles) exhibit significant surface roughness and typically have a relatively steep gradient compared to the pools.

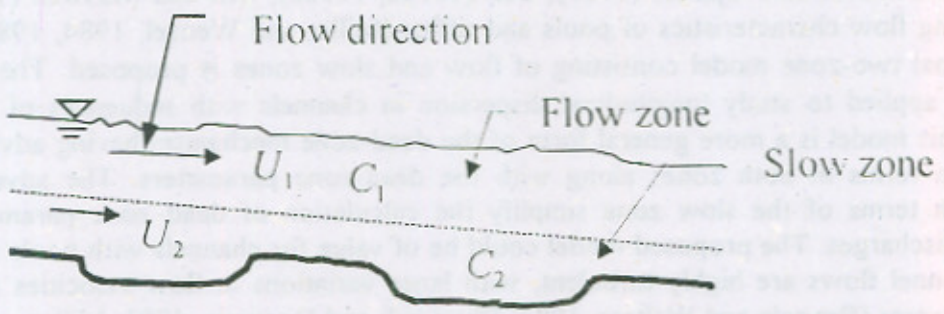

Fig. 1 Sketch of pools and riffles in a natural channel, showing average velocity and concentration in flow and slow zones.

This study is confined to slow zones adjoining the channel bed, but the trapping may occur due to slow zones associated with channel sides. In principle, however, the model given below, with suitable reinterpretation, could be applied to flows with side slow zones.

Denoting the cross-sectional average solute concentration in zone n at the longitudinal spatial co-ordinate x at time t by $C_n(x,t)$, the evolution and interaction of these

concentrations is modeled via two advection-dispersion equations, coupled by a mass exchange term:

$$A_n \frac{\partial}{\partial t} C_n = -\frac{\partial}{\partial x}(U_n A_n C_n) + \frac{\partial}{\partial x}\left(D_n A_n \frac{\partial}{\partial x} C_n\right) \pm m\Delta C \qquad n = 1,2 \qquad (1)$$

In this equation, $A_n(x)$ denotes the cross-sectional area (m^2) of the flow in zone n at the point x. Similarly $U_n(x)$ and $D_n(x)$ denote, respectively, the mean fluid velocity (m/s) and longitudinal dispersion coefficient (m^2/s) in zone n. In the final term on the right-hand side of equation (1) $\Delta C = C_2 - C_1$, and m denotes the mass exchange coefficient per unit length (m^2/s) at the interface of two zones. Hence, the sign preceding this last term is positive for $n = 1$ and negative for $n = 2$.

It may be noted that the model expressed by equation (1) constitutes a generalization of the two zone mechanism and allows for the variations in hydraulic parameters in both zones, and also for advective and dispersive transport in the slow zone. If we assume average slow zone velocity to be zero and neglect the dispersion term then this two-zone model reduces to a simple one-dimensional advection-dispersion model with dead zone parameters. This two zone mechanism also converges to a classical Fickian type advection-dispersion equation when the slow zone area diminishes. The experimental results presented below indicate that longitudinal advection could be a significant transport mechanism in the slow zones, and could be accounted for in any dispersion model.

Assuming, at $t = 0$, a mass M^* of solute is introduced uniformly across the flow area at $x = 0$, the corresponding initial conditions for equation (1) are

$$C_n(x,0) = c_0 \delta(x) \qquad n = 1,2 \qquad (2)$$

where $c_0 = M^* / (A_1(0) + A_2(0))$ at the $x = 0$, and $\delta(x)$ is the Dirac delta function. Appropriate far field conditions for equation (1) are then

$$C_n(x,t) = \rightarrow 0 \qquad \text{as } |x| = \rightarrow \infty, \qquad t \geq 0 \qquad n = 1,2 \qquad (3)$$

The following implicit finite-difference numerical approach is employed to study the model given by equations (1), (2), and (3). Uniformly spaced grid points $(x_i, t_k) = (i\delta x, k\delta t)$, $i = -M, \ldots, +N$, $k = 0,1,\ldots,K$, are introduced, where δx and δt define distance and time steps respectively, and the integers K, M and N define the domain over which the computation is to be performed.

Following Stone and Brian (1963) the grid point values of the concentration time derivatives are approximated using

$$\frac{\partial}{\partial t} C_i^k \approx \Delta_t^+ \left(\frac{1}{6} C_{i-1}^k + \frac{2}{3} C_i^k + \frac{1}{6} C_{i+1}^k\right) \qquad (4)$$

where $C(x_i, t_k) = C_i^k$ (C is either C_1 or C_2), and where Δ_t^+ is the forward difference operator, $\Delta_t^+ C_i^k = (C_i^{k+1} - C_i^k) / \delta t$.

To accommodate gradients generated by variations of cross-sectional area of flow and slow zones in channels with pools and riffles, it is appropriate to expand spatial derivatives of equation (1) using the Chain rule

$$\frac{\partial}{\partial x}(QC) = Q\frac{\partial}{\partial x}C + C\frac{\partial}{\partial x}Q \tag{5}$$

where $Q = U_n A_n$

and the gradients are then approximated by

$$\frac{\partial}{\partial x}C_i^k \approx \frac{1}{2}\Delta_x^0\left(C_i^{k+1} + C_i^k\right) \quad \text{and} \quad \frac{\partial}{\partial x}Q_i \approx \Delta_x^+ Q_i \tag{6}$$

where Δ_x^0 and Δ_x^+ are the central and forward difference operators respectively; $\Delta_x^0 C_i^k = (C_{i+1}^k - C_{i-1}^k)/2\delta x$ and $\Delta_x^+ Q_i = (Q_{i+1} - Q_i)/\delta x$. A similar procedure is adopted for the dispersive terms, and the standard Crank-Nicholson approximation is used for $\partial^2 C/\partial x^2$. Following Seo (1990a) the mass exchange term of equation (1) is discretized as

$$\Delta C_i^k \approx C_{1,i}^k - C_{2,i}^k \tag{7}$$

Corresponding to equation (2) the initial condition for the numerical scheme is $C_{n,0}^0 = c_{n,0}\,\delta x$, and corresponding to equation (3) the boundary conditions are $C_{n,-M}^k = C_{n,N}^k = 0, \quad k \geq 0$.

The resulting system of linear equations for $C_{n,i}^k = C_n(x_i, t_k)$ is written in the following block matrix form

$$\begin{pmatrix} A^{(1)} & B^{(1)} \\ B^{(2)} & A^{(2)} \end{pmatrix}\begin{pmatrix} \underline{c}_1^{k+1} \\ \underline{c}_2^{k+1} \end{pmatrix} = \begin{pmatrix} P^{(1)} & 0 \\ 0 & P^{(2)} \end{pmatrix}\begin{pmatrix} \underline{c}_1^{k} \\ \underline{c}_2^{k} \end{pmatrix} \tag{8}$$

where $\underline{c}_n^k = (C_{n,-M}^k, \ldots, C_{n,N}^k)^T$. The blocks $A^{(i)}$, $P^{(i)}$ are tridiagonal matrices, and the $B^{(i)}$ are diagonal matrices. We omit the algebraic details of the construction of (8), which are straight-forward. The linear system given by (8) is solved using the following block Gauss-Siedel iterative scheme at each time-step:

$$A^{(1)}\Gamma_1^{(\nu+1)} = P^{(1)}\underline{c}_1^k - B^{(1)}\Gamma_2^{(\nu)} \tag{9}$$

$$A^{(2)}\Gamma_2^{(\nu+1)} = P^{(2)}\underline{c}_2^k - B^{(2)}\Gamma_1^{(\nu+1)} \tag{10}$$

where $\Gamma_n^{(\nu)}$ is the $\nu-$th iteration approximation to $\underline{c}_n^{k+1}$ (with $\Gamma_n^{(0)} = \underline{c}_n^k$). Since $A^{(1)}$ and $A^{(2)}$ are constant, tri-diagonal matrices, the solution of equations (9) and (10) are easily obtained, making use of upper and lower triangular decomposition of $A^{(1)}$ and $A^{(2)}$ (Press et al., 1992).

Before using this numerical approach to study the two-zone model for geometries of interest it is important to assess the effectiveness of the method itself. This is presented in the following section, making use of known analytical solutions.

COMPARISON OF NUMERICAL AND ANALYTICAL SOLUTIONS

With $D_1 = D_2 = D$, U_n and A_n independent of x, the model given by equation (1) simplifies to

$$\frac{\partial}{\partial t}C_n = -U_n\frac{\partial}{\partial x}C_n + D\frac{\partial^2}{\partial x^2}C_n \pm \varepsilon\beta_n\Delta C \qquad , \; n = 1,2 \qquad (11)$$

where $\varepsilon = m/(A_1 + A_2)$ is a normalized mass exchange coefficient and $\beta_n = (A_1 + A_2)/A_n$ is the reciprocal of the normalized cross-sectional area of zone n.

Equations (11) together with the conditions given by expressions (2) and (3) have an analytical solution, (see Chikwendu and Ojiakor, 1985), and the efficiency and effectiveness of the numerical approach described in the previous section has been assessed by reference to this solution. Figs. 2 and 3 show results that demonstrate the ability of the numerical method to accurately resolve both spatial and temporal variations in concentration profiles. Fig. 2 shows the time variation of the sectional-average concentration $C_0 = \eta_1 C_1 + \eta_2 C_2$ at four fixed locations, while Fig. 3 shows the spatial variation of C_0 at five time points. Here $\eta_n = A_n/(A_1 + A_2)$ is the normalized area of zone n.

The flow parameters used to obtain these results were $U_1 = 1$, $U_2 = 0.1$, $D = 1$, $m = 0.001$, $A_1 = 0.75$, $A_2 = 0.25$. (These values are not typical of real flows but were used to demonstrate the capability of the numerical method to resolve the large gradients observed in these solutions). Values of the numerical parameters used to produce the results of Figs. 2 and 3 were $\delta x = 0.5$ and $\delta t = 0.3$.

Figs. 4 and 5 show how the first two temporal moments of the concentration C_0 vary with position: Fig. 4 depicts the mean travel time

$$T(x) = \frac{\int_0^\infty tC_0(x,t)dt}{\int_0^\infty C_0(x,t)dt} \qquad (12)$$

for a range of values of the velocity ratio U_2/U_1, and Fig. 5 shows corresponding results of the temporal variance

$$T''^2(x) = \frac{\int_0^\infty (t - T)^2 C_0(x,t)dt}{\int_0^\infty C_0(x,t)dt} \qquad (13)$$

The parameter values used to compute these results were $U_1 = 1$, $U_2/U_1 = 0.25$, 0.5, 0.75, $A_1 = 0.60$, $A_2 = 0.40$, $D = 1$, $m = 0.001$. Again there is good agreement between numerical and analytical results. These results (Figs. 4 & 5) also demonstrate the significance of the velocity ratio (U_2/U_1) to longitudinal dispersion. The mean travel time and temporal variance progressively increased with the decrease in velocity ratio. In the following section the numerical results of the model are compared to the laboratory experimental data.

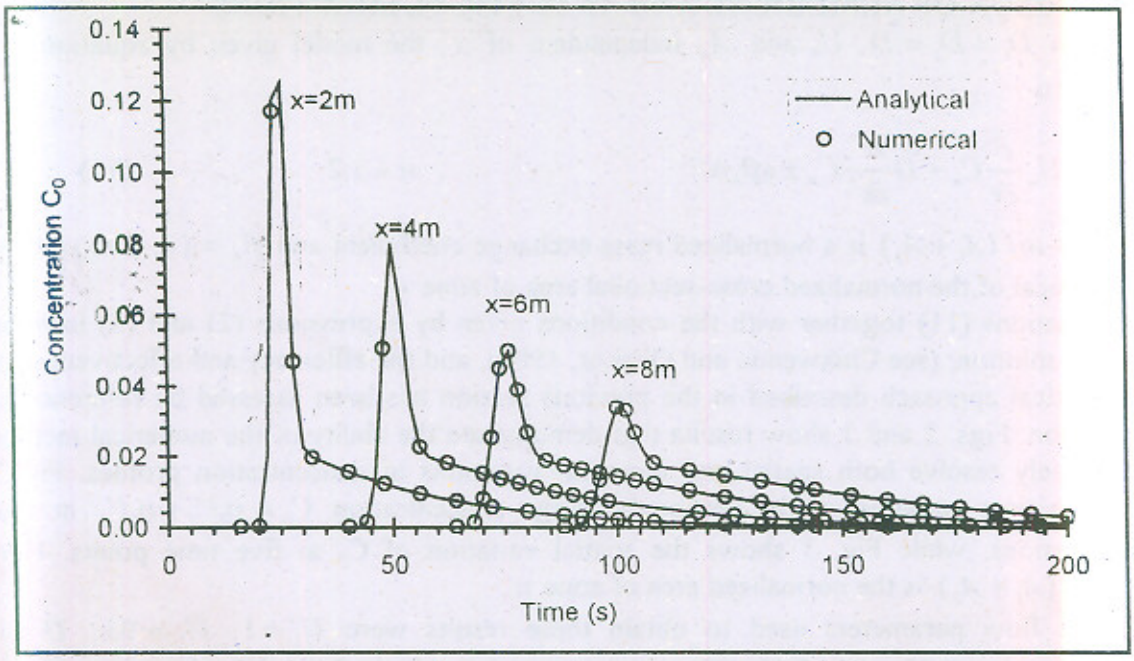

Fig. 2 Analytical and numerical concentration-time profiles.

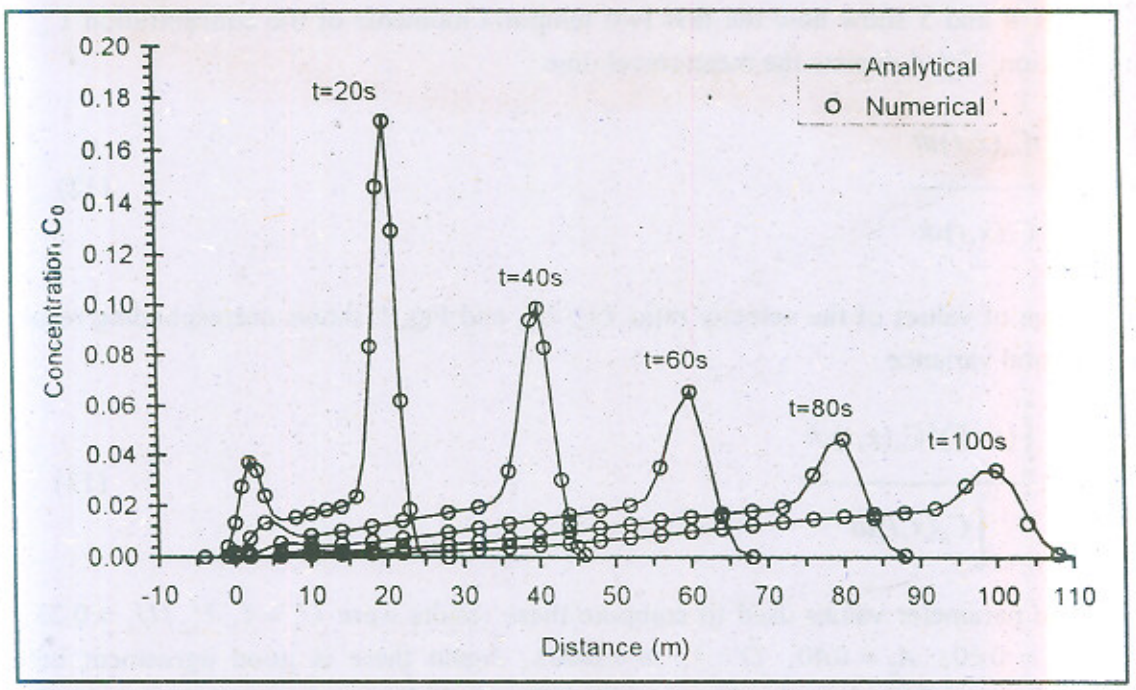

Fig. 3 Analytical and numerical concentration-distance profiles

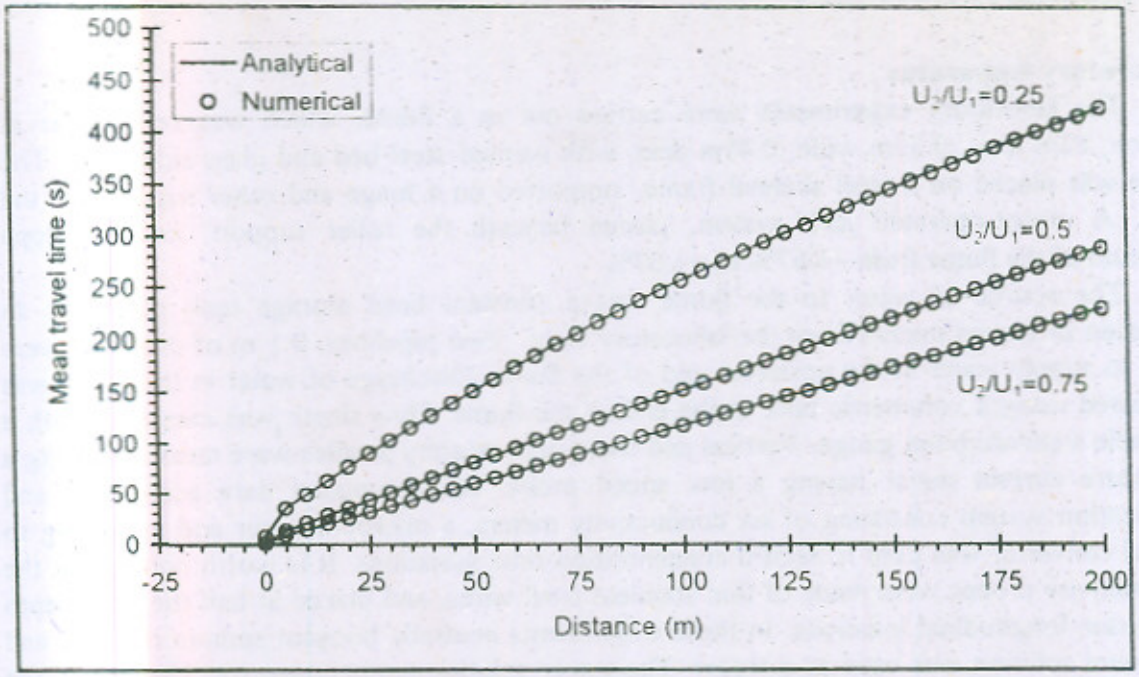

Fig. 4 Analytical and numerical mean travel time.

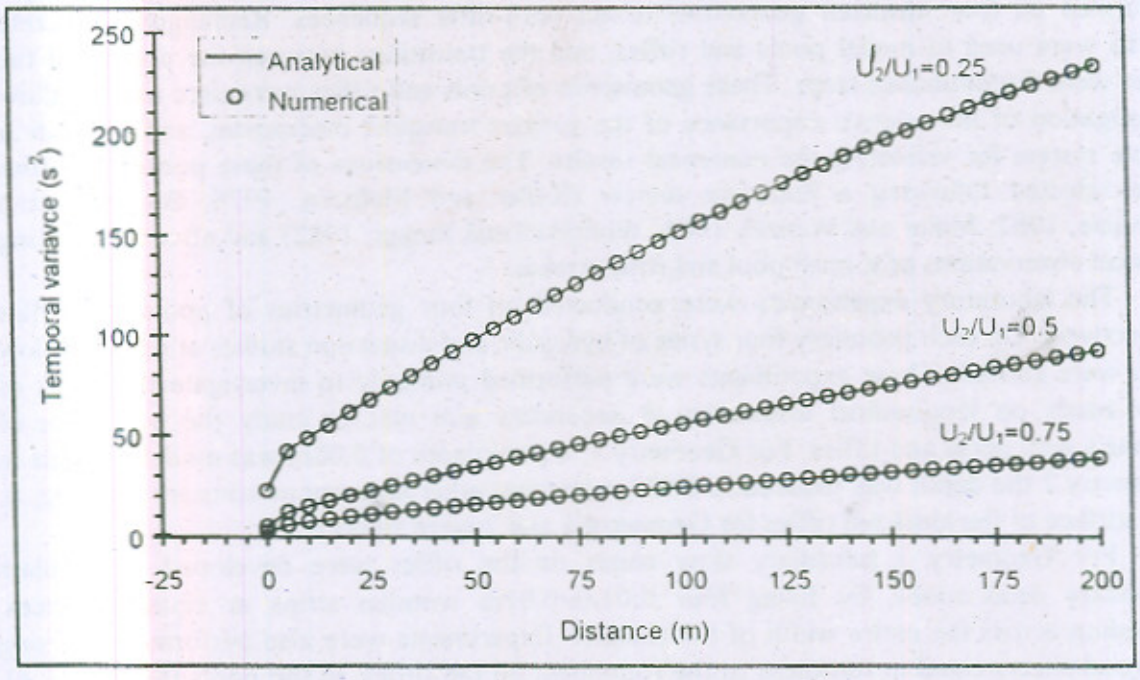

Fig. 5 Analytical and numerical temporal variance.

EXPERIMENTAL STUDIES

Laboratory Apparatus

The laboratory experiments were carried out in a flume, which was rectangular in section, 12m long, 0.31m wide, 0.45m deep with painted steel bed and glass side walls. The flume was placed on a steel skeletal frame, supported on a hinge and roller supports at the ends. A motor-operated jack system, placed beneath the roller support, enabled slope variation of the flume from −1.67% to +1.67%.

The source of water to the flume was a constant head storage tank placed at an elevation of eleven meters from the laboratory floor. Two pipelines, 0.1 m of diameter were used to supply water at the upstream end of the flume. Discharge of water in the flume was measured using a volumetric tank at the end of the flume. Flow depth was measured with a movable standard point gauge. Vertical and transverse velocity profiles were measured using a miniature current meter having a low speed probe. An automated data acquisition and digitization system consisting of six conductivity meters, a microcomputer and an analog to digital converter was used to record concentration-time variations. It is worth noting that the conductivity probes were made of thin stainless steel wires, and placed at half the flow depth at chosen longitudinal locations. In these experiments neutrally buoyant sodium chloride and methanol solution was used as a tracer. The tracer solution temperature was brought to the flume water level by immersing the solution container in a water tank.

Bed Form Geometries and the Experimental Plan

To calibrate and validate the two-zone dispersion model, and to develop an improved understanding of hydraulics of channels with pools and riffles, laboratory experiments were performed on four idealized geometries of six pool-riffle sequences. Rectangular concrete blocks were used to model pools and riffles, and the transitions between the pools and the riffles were discontinuous steps. These geometries of pools and riffles were used as they allow investigation of the relative importance of the various transport mechanism, and provide a simple system for validating the numerical results. The dimensions of these pools and riffles were selected following a literature review (Keller and Melhorn, 1978; Bhowmik and Demissie, 1982; Miller and Wenzel, 1985; Whittaker and Jaeggi, 1982) and after undertaking physical observations of a small pool and riffle stream.

The laboratory experiments were conducted on four geometries of pools and riffles respectively. On each geometry four series of hydraulic and dispersion studies at different flow rates were carried. These experiments were performed primarily to investigate the effect of slow zones on longitudinal dispersion. A secondary aim was to study the hydraulics of channels with pools and riffles. For Geometry 1, a pool depth of 0.06m was modeled, while in Geometry 2 the depth was reduced to 0.035m keeping other dimensions constant. See Fig. 6. The surface of the idealized riffles for Geometry 1 and 2 were smooth.

For Geometry 3 subsidiary slow zones on the riffles were developed to simulate secondary dead zones, by fixing four 0.01m×0.01m wooden strips at equal distances, extending across the entire width of the channel. Experiments were also performed by fixing plywood sheets equal in thickness to the roughness on the riffles, in the pools (Geometry 4). In all the laboratory experiments the flume bed slope was the same (0.625%). Fig. 6 shows the geometries used to perform the laboratory experiments.

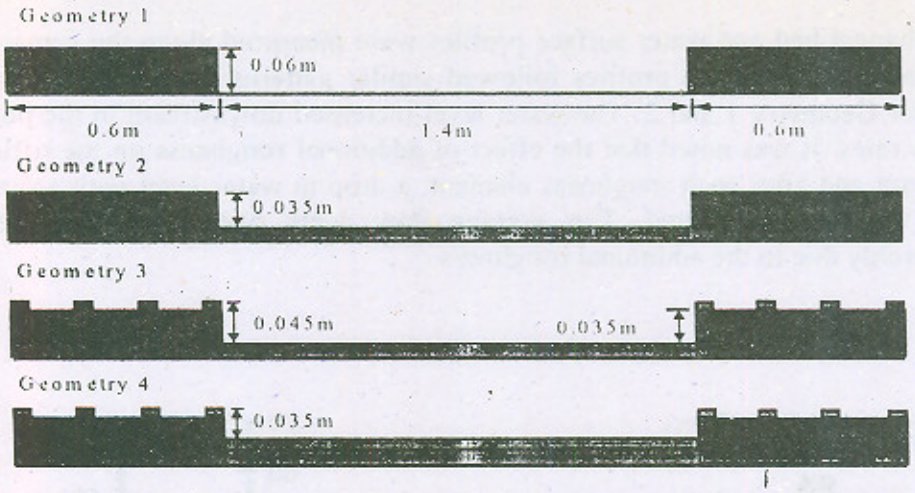

Fig. 6 Geometries of idealized pools and riffles modeled in the laboratory flume.

Hydraulic Studies

To study the hydraulics of channels with pools and riffles and to provide parameter values for the two-zone transport model, depths of flow and velocity profiles were measured. Water surface and bed profiles were measured along the centerline of the flume. Vertical velocity profiles were measured at stations S1 to S5, as shown in Fig. 7, while transverse velocity profiles at half the flow depths were measured at S3, S4 and S5, in a typical pool-riffle sequence.

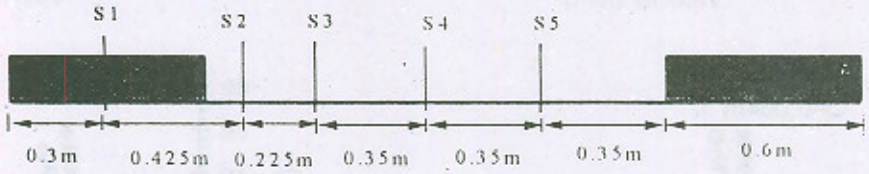

Fig. 7 Velocity measurement stations in a typical pool-riffle sequence.

Vertical velocity profiles were almost uniform over smooth riffles, while gradients in the velocity profiles were observed over the riffles having additional roughness. Steep gradients in the vertical velocity profiles were found at S2, which was 0.125m from the upstream end of the pool. Recirculation zones were observed at the upstream end of these idealized pools of Geometry 1, 3 and 4 for all flow rates. No recirculation of water was noted in pools of Geometry 2. The magnitude of velocities decreased downstream of the pools with an increase in flow depths. Average slow zone velocities in the pools also increased progressively with the increase in discharge for all experiments. The vertical velocity profiles for Geometry 2 experiments are shown in Fig. 8.

In the measurement of the transverse velocities a considerable amount of turbulence was observed. At the start of the pools the profiles did not follow the conventional logarithmic shape. At S4 and S5 the velocity profiles were fairly uniform with less turbulence. The flow in the laboratory flume was turbulent (Reynolds number varied from 4200-15000 for the flow rates studied) and non-uniform with large fluctuations in the velocity values.

Channel bed and water surface profiles were measured along the centerline of the flume. Water surface profiles followed similar patterns over the pools and the riffles for Geometry 1 and 2. The water level increased downstream in the pools for all flow rates. It was noted that the effect of additional roughness on the riffles was significant and after each roughness element, a drop in water level with an increase in the velocity was found. The average flow depth over the riffles increased considerably due to the additional roughness.

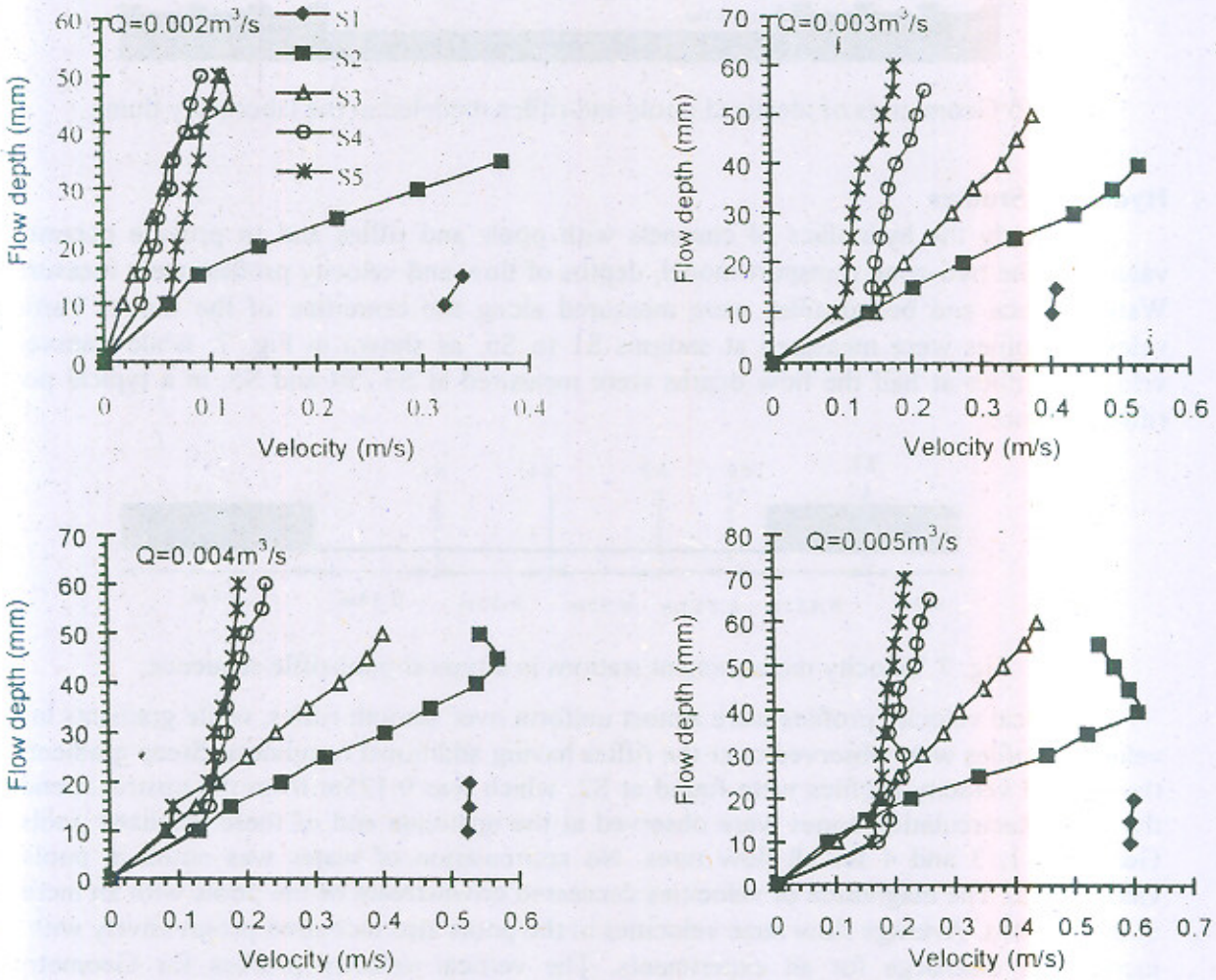

Fig.8 Vertical velocity profiles in a typical pool-riffle sequence. (Geometry 2)

COMPARISON OF THE EXPERIMENTAL AND THE NUMERICAL SOLUTIONS

To validate parameters of the two-zone model, series of systematic longitudinal dispersion experiments were performed on four geometries of pools and riffles. However, in this paper the results of two series of Geometry 1 and 2 are presented.

To assess the individual effects of pools and riffles, concentration-time profiles were recorded at 1.4 m and 0.6 m intervals, corresponding to the upstream and downstream end of the riffles. The data were recorded at eleven stations, injecting a known quantity of the tracer solution at the upstream of the first riffle as a line source across the flume. Number of dispersion runs were performed using the same quantity of tracer solution at the same hydraulic conditions. Runs average concentration-time profiles (called series) were used to compute the statistical parameters such as mean travel time, temporal variance, skew, mean velocity and longitudinal dispersion coefficients, which were compared with the simulated values.

Table 1 presents the input values of the hydraulic parameters, vertical velocities, flow depths and the discharge, used in the two-zone model. Flow depths were measured at a number of points along the centerline of the flume. Slow zone depths were measured from the bottom of the flume to the height of roughness on the riffles. Velocities in flow and slow zones in the pools were computed by averaging the vertical velocity profiles measured at various stations. Flow and slow zone velocities on the riffles were computed in a similar fashion. It is worth noting that there was a considerable increase in average slow zone velocities with the increase in flow rates for all data sets.

The values of mass exchange coefficients used in numerical simulations are presented in Table 2, which were approximately the same as those measured experimentally for Geometry 1-5 (Appendix C). The non-dimensional simulated exchange coefficient k^* varied from 0.027 to 0.0315. These values were higher than the non-dimensional value 0.02 proposed by Valentine and Wood (1977) and lesser than the values reported by Seo (1990a) and the values computed in this study for higher pool lengths (Appendix C). This variation emerged due to advection and dispersion terms employed in the slow zone of two-zone model.

Various empirical relations of longitudinal dispersion coefficients for open channel flow had already been developed considering vertical and transverse velocity variations and turbulence (Elder, 1959; Fischer, 1967; Chikwendu and Ojiakor, 1985). However, the dispersion coefficients employed in this two-zone model were for uniform, open-channel flow in a flume with smooth bed and glass side walls. A number of numerical tests were carried out to select an appropriate value of the dispersion coefficient. The value was selected fitting simulated curves to rising sides of concentration-time profiles. The dispersion coefficient 0.002 m^2/s for both flow and slow zones produced reasonably comparable profiles to measured data. The dimensionless values of dispersion coefficients ($0.002/h_n U_*$) were also found near to the non-dimensional dispersion coefficient $0.0048/\kappa^3$ proposed by Chikwendu and Ojiakor (1985).

Figs. 9 and 10 show experimental and numerical concentration-time profiles of Series 1 and 2 (Geometry 1). As shown in these figures the agreement between measured and numerical concentration profiles improved along the downstream of the flume. The simulated concentration profiles showed prolonged tails, having consistency to measured data. In Series 1, the experimental and numerical peak concentration decayed as a function of $t^{-0.83}$ and $t^{-0.88}$ between 2 m and 4 m from the tracer injection, respectively. The experimental and numerical

peak concentration decayed as a function of $t^{-0.49}$ and $t^{-0.53}$ between 8 m and 10 m from the tracer injection. The peak concentration difference and time to peak difference between measured and numerical values at 10 m were 2.5% and 3.5%, respectively.

Figures 11 and 12 show the mean travel time and temporal variance of measured and simulated data. A stair like change in mean travel time and temporal variance showed the contribution of pools and riffles on longitudinal dispersion mechanism. The simulated curves showed a linear increase in mean travel time and temporal variance, which were consistent to the measured data. In this data set, the effect of smooth riffles on longitudinal dispersion was negligible.

For Geometry 2 the depth of pools was reduced from 0.06 m to 0.035m keeping other dimensions intact. The hydraulic and other input parameters to numerical solutions are given in tables 1 and 2. Figs. 13 and 14 show experimental and numerical concentration-time profiles of Series 3 and 4 (Geometry 2). Skewed and prolong tails of the simulated concentration profiles were consistent to the measured data. The peak concentration difference and time to peak difference between measured and numerical values at 10 m from the tracer injection were 6.211% and 1.25%, respectively (Series 3, Geometry 2). The experimental and numerical peak concentration decay rate eventually reduced along the flume in downstream direction.

Figs. 15 and 16 show mean travel time and temporal variance of measured and simulated data. The profiles showed linear increase in mean travel time and temporal variance having different slopes on pools and riffles. The numerical results were in agreement with the observed values. However, the values of mean travel time and temporal variance were less than of Geometry 1. This was due to decrease in slow zone area of the pools and increase in average velocity of slow zones.

Table 3 presents mean cloud velocity ($\overline{U}_{cloud}$) and overall longitudinal dispersion coefficient (K_x) of measured and simulated concentration-time data of Series 1 and 2 (Geometry 1) and Series 3 and 4 (Geometry 2). The measured and simulated $\overline{U}_{cloud}$ showed variance of 2.2% and 5.47% in Series 1 and 2 (Geometry 1). The longitudinal dispersion coefficient (K_x) also showed difference of 9.14% and 11.31% in Series 1 and 2 (Geometry 1). Similar variations in mean cloud velocity and longitudinal dispersion coefficients were noted for other geometries. The $\overline{U}_{cloud}$ increased with the increase in discharge. The values also increased by the decrease in pool depth. The longitudinal dispersion coefficient (K_x) increased with the increase in pool depth and discharge.

Geometry	Series	Q m^3/s	Flow depth in Pool (m)		Flow Depth on Riffle (m)		Velocity in Pool (m/s)		Velocity on Riffle (m/s)	
			Zone 1	Zone 2	Zone 1	Zone 2	Zone 1	Zone 2	Zone 1	Zone 2
1	1	0.002	0.023	0.06	0.02	0	0.22	0.023	0.33	----
	2	0.003	0.028	0.06	0.024	0	0.287	0.066	0.41	----
2	3	0.004	0.032	0.035	0.033	0	0.31	0.082	0.4	----
	4	0.005	0.035	0.035	0.035	0	0.35	0.10	0.48	----

Table 1 Hydraulic parameters used in numerical solution.

Geometry	Series	Q m^3/s	m (m^2/s)	$k^* = m / wU^*$	D (m^2/s)
1	1	0.002	0.0019	0.027	0.002
	2	0.003	0.0031	0.0315	0.002
2	3	0.004	0.0026	0.029	0.002
	4	0.005	0.0029	0.029	0.002

U^*: average flow zone velocity of the pool

Table 2 The dispersion and mass exchange coefficients employed in numerical solutions.

	Geometry 1		Geometry 2	
Flow Rate	(Series 1)	(Series 2)	(Series 3)	(Series 4)
$\overline{U}_{cloud}$ (exp) m/s	0.1091	0.1460	0.2392	0.2866
$\overline{U}_{cloud}$ (simu)m/s	0.1067	0.1380	0.2319	0.2743
K_x(exp) m^2/s	0.0350	0.0389	0.0283	0.0334
K_x(simu)m^2/s	0.0318	0.0433	0.0211	0.0264

exp: experimental

simu: simulated

Table 3 Experimental and simulated values of mean velocity and longitudinal dispersion coefficients of concentration-time profiles.

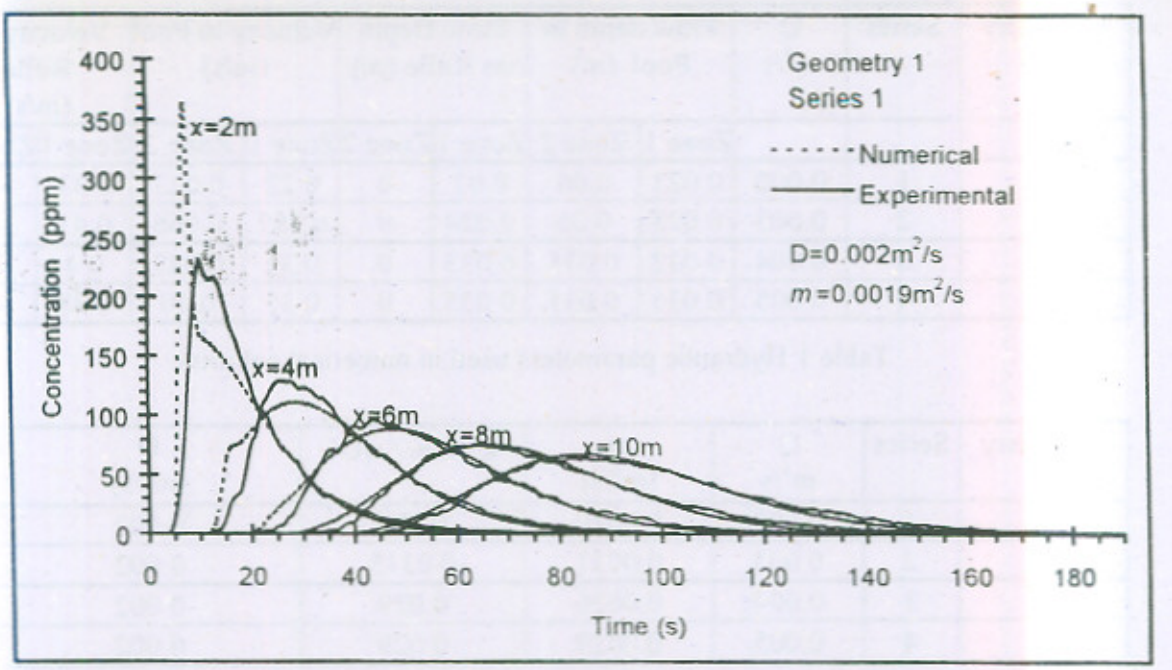

Fig. 9 Experimental and numerical concentration-time profiles.

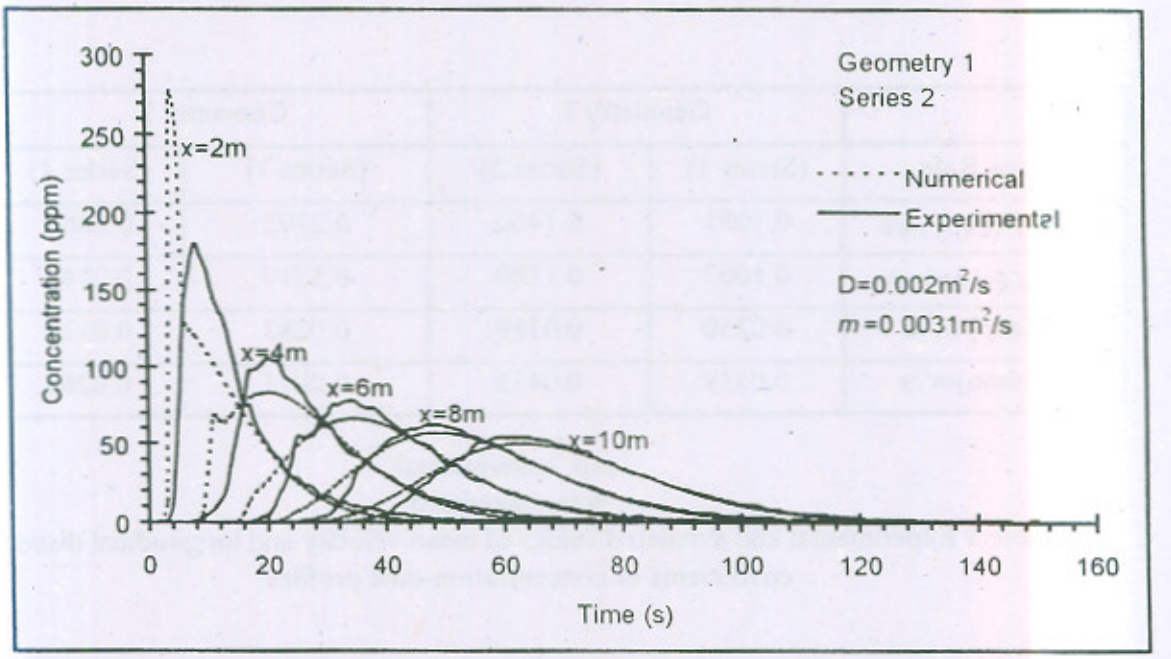

Fig. 10 Experimental and numerical concentration-time profiles.

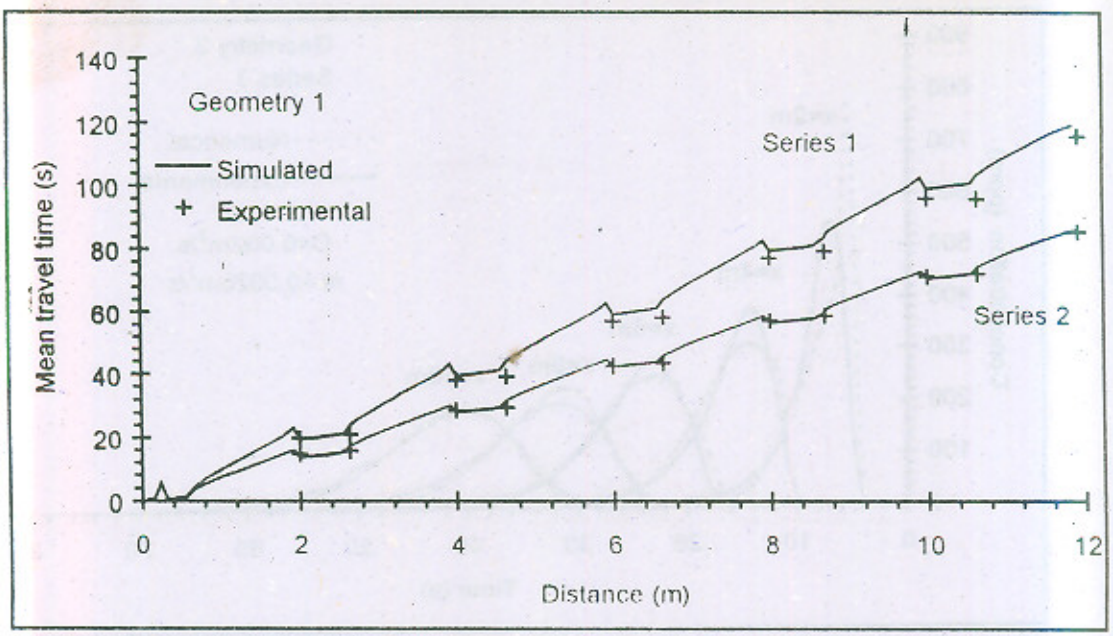

Fig. 11 Experimental and numerical mean travel time. Series 1 and 2 (Geometry 1)

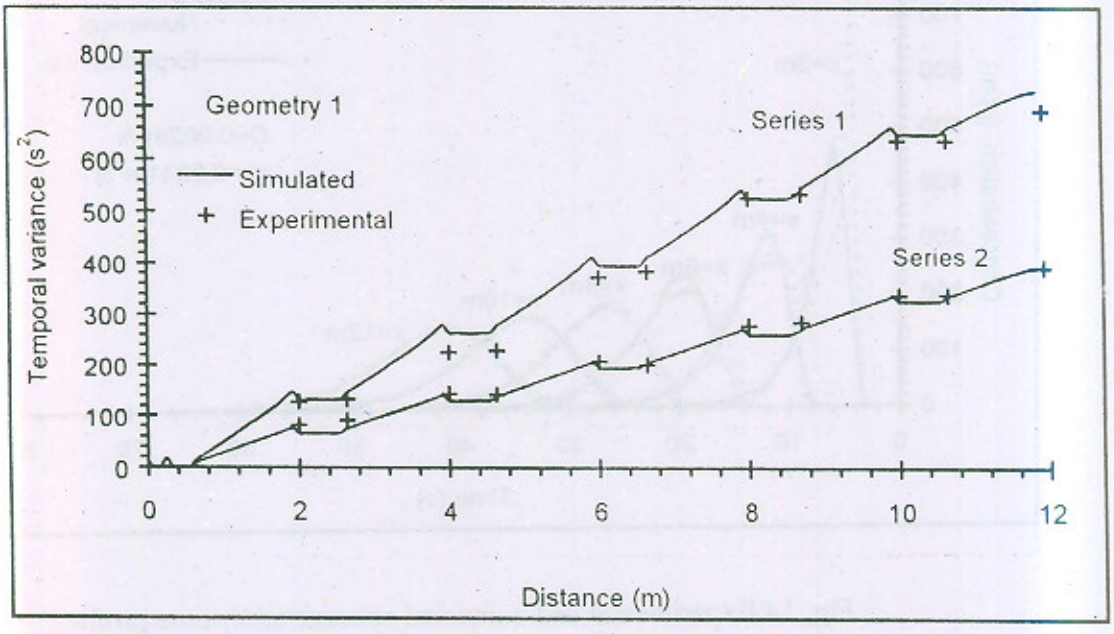

Fig. 12 Experimental and numerical temporal variance. Series 1 and 2 (Geometry 1)

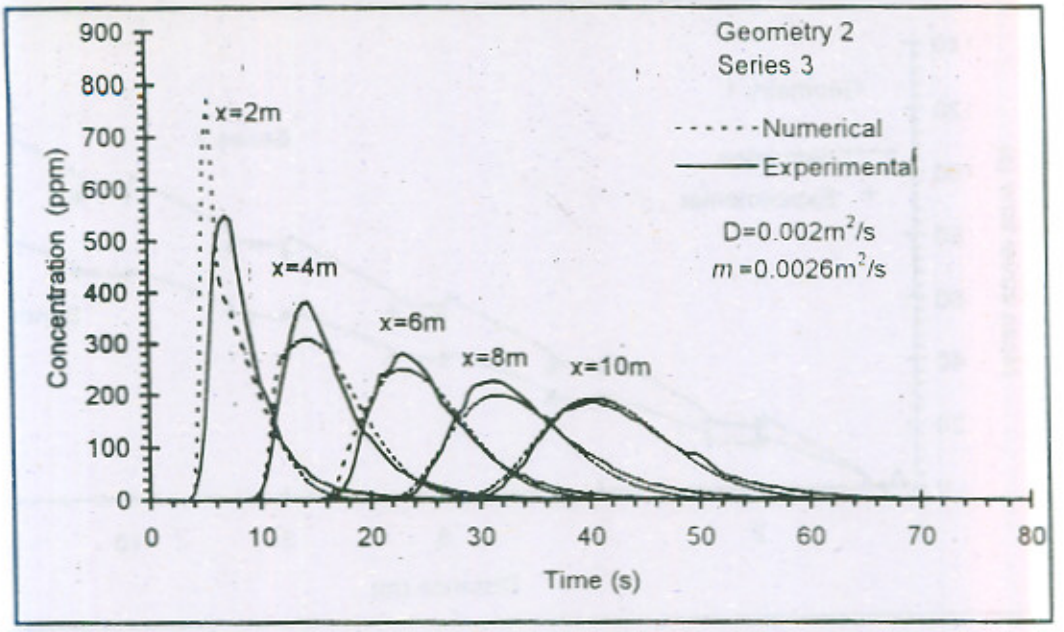

Fig. 13 Experimental and numerical concentration-time profiles.

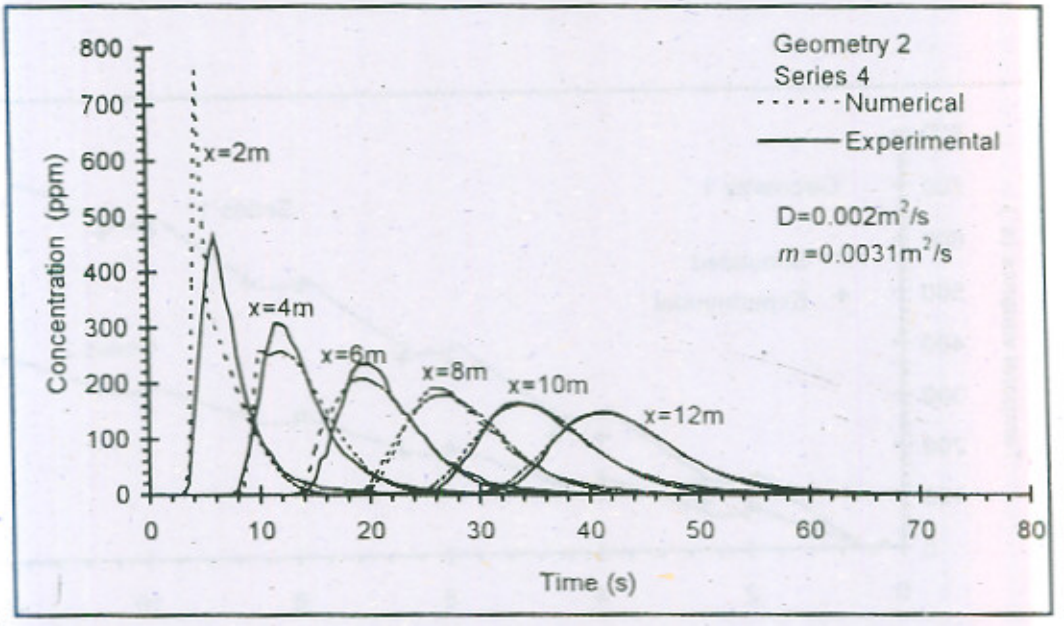

Fig. 14 Experimental and numerical concentration-time profiles.

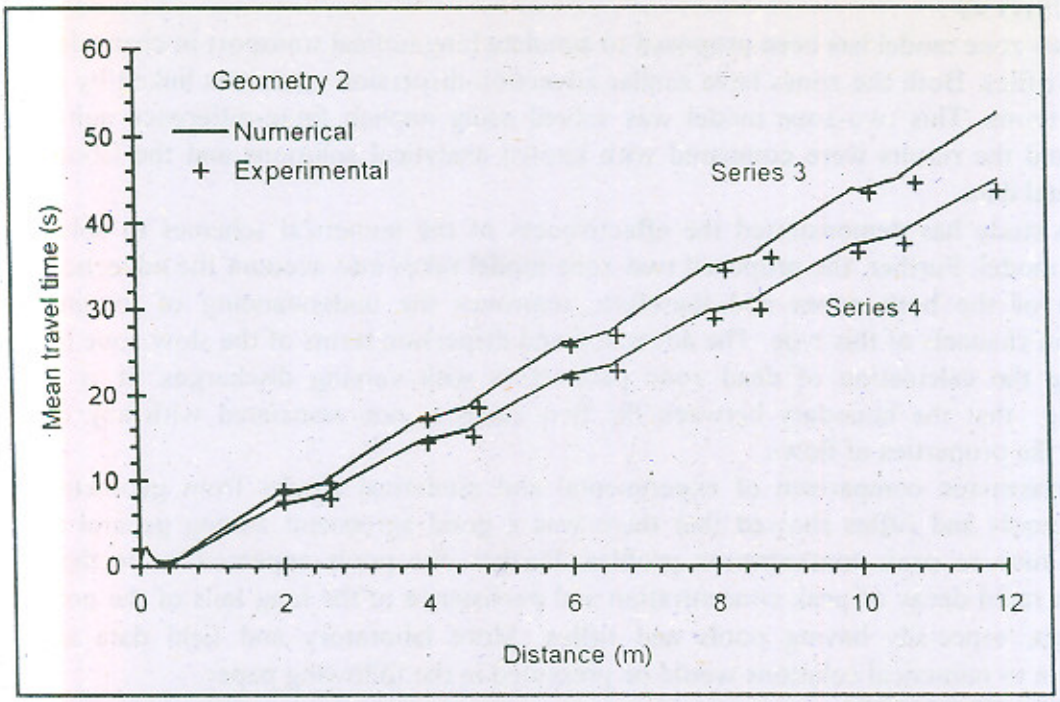

Fig. 15 Experimental and numerical mean travel time. Series 3 and 4 (Geometry 2)

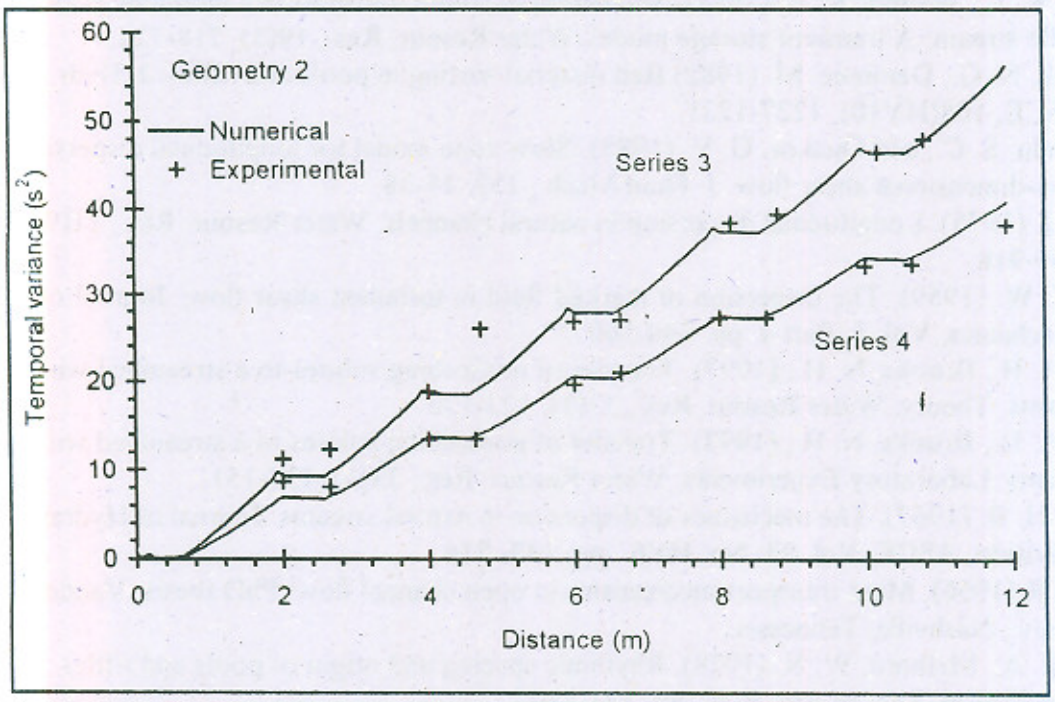

Fig. 16 Experimental and numerical temporal variance. Series 3 and 4 (Geometry 2)

CONCLUSIONS

A two-zone model has been proposed to simulate longitudinal transport in channels with pools and riffles. Both the zones have similar advection-dispersion equations linked by mass-exchange terms. This two-zone model was solved using implicit finite-difference numerical schemes and the results were compared with known analytical solutions and the laboratory experimental data.

This study has demonstrated the effectiveness of the numerical schemes to solve the two-zone model. Further, the proposed two-zone model takes into account the advection and dispersion of the both zones and therefore, improves the understanding of longitudinal transport in channels of this type. The advection and dispersion terms of the slow zone help in simplifying the calculation of dead zone parameters with varying discharges. It is worth mentioning that the boundary between the two zones is not associated with any drastic change in the properties of flows.

A systematic comparison of experimental and numerical results from geometries of idealized pools and riffles showed that there was a good agreement among general shape, peak and time to peak concentration profiles. Further, the pools appeared to be the main reason for rapid decay of peak concentration and persistence of the long tails of the pollutant in channels, especially having pools and riffles. More laboratory and field data and its comparison to numerical solutions would be presented in the following paper.

ACKNOWLEDGMENT

The Ministry of Education, Govt. of Pakistan supported the first author for the duration of this study.

APPENDIX A. REFERENCES

Bencala, K. E., Walters, R. A. (1983). Simulation of solute transport in a mountain pool-and-riffle stream: A transient storage model. Water Resour. Res., 19(3), 718-724.

Bhowmik, N. G., Demissie. M. (1982) Bed material sorting in pools and riffles. J. Hydr. Div., ASCE, 108(HY10), 1227-1231.

Chikwendu, S. C., and Ojiakor, G. V. (1985). Slow zone model for longitudinal dispersion in two-dimensional shear flow. J. Fluid Mech., 152, 15-38.

Day, T. J. (1975). Longitudinal dispersion in natural channels. Water Resour. Res., 11(9), 909-918.

Elder, T. W. (1959). The dispersion of marked fluid in turbulent shear flow. Journal of Fluid Mechanics, Vol. 5, Part 4. pp. 544-560.

Elliott, A. H., Brooks, N. H., (1997). Transfer of nonsorbing solutes to a streambed with bed forms: Theory. Water Resour. Res., 33(1), 123-136.

Elliott, A. H., Brooks, N. H., (1997). Transfer of nonsorbing solutes to a streambed with bed forms: Laboratory Experiments. Water Resour. Res., 33(1), 137-151.

Fischer, H. B. (1967), The mechanics of dispersion in natural streams. Journal of Hydraulics Division, ASCE, Vol. 93. No. HY6, pp. 187- 216.

Hays, J. R.(1966). Mass transport mechanisms in open channel flow. PhD thesis, Vanderbuilt Univ., Nashville, Tennessee.

Keller, E. A, Melhorn, W. N. (1978). Rhythmic spacing and origin of pools and riffles. Geological. Soc. of Am. Bull., 89, 723-730.

Miller, B. A., Wenzel, H. G. (1985). Analysis and simulation of low flow hydraulics. J. Hydr. Engrg., 111(12), 1429-1446.

Press, W. H., Teukolsky, S. A., Vetterling, W. T., and Flannery, B. P., (1992). Numerical Recipes in FORTRAN, 2nd Ed, Cambridge University Press.
Sear, D. A., (1996). Sediment transport processes in pool-riffle sequences. Earth Surface Processes and Landforms, Vol. 21, pp. 241-262.
Seo, I. W. (1990). Low flow mixing in open channels. PhD Thesis., Univ. of Illinois at Urbana-Champaign, Urbana, Illinois.
Seo, I. W. (1990). Laboratory and numerical investigation of longitudinal dispersion in open channels. Water Resour. Bull., 26(5), 811-821.
Seo, I. W., Maxwell, W. H. C. (1992). Modelling low-flow mixing through pools and riffles. J. Hydr. Engrg., 118(10), 1406-1423.
Smith, R. (1976). Longitudinal dispersion of a buoyant contaminant in a shallow channel. J. Fluid Mech., 78, 677-688.
Smith, R. A. (1979). A delay-diffusion description for contaminant dispersion. J. Fluid Mech., 105, 469-486.
Stone, H. L., Brian, P. L. T. (1963). Numerical solution of convective transport problems. A.I.Ch.E. Journal., 9(5), 681-688.
Taylor, G. I. (1954). The dispersion of matter in turbulent flow through a pipe. Proc. Royal Soc., London, 233, 446-468.
Thackston, E. L., Schnelle, K. B. (1970). Predicting effects of dead zones on stream mixing. J. Sanitary Engrg., ASCE, 96, 319-331.
Tsai, Y. H., and Holley, E. R. (1979). Temporal and spatial moments for longitudinal mixing in prismatic channels with storage in separation zones. Hydraulic Engieering Series, No. 35, University of Illinois, Urbana, Illinois.
Valentine, E. M., and Wood, I. R. (1977). Longitudinal dispersion with dead zones. J. Hydr. Div., ASCE, 105(HY9), 975-990.
Valentine, E. M., and Wood, I. R. (1979). Experiments in longitudinal dispersion with dead zones. J. Hydr. Div., ASCE, 105(HY8), 999-1016.
Valentine, E. M., and Wood, I. R. (1979). Dispersion in rough rectangular channels. J. Hydr. Div., ASCE, 105(HY12), 1537-1553.
Whittaker, J. G., Jaeggi, M. N. R. (1982). Origin of step-pool systems in mountain streams. J. Hydr. Engrg., 108(6), 758-773.
Young, P.C., and Wallis, S.G., (1993). Solute transport and dispersion in stream channels. In: Channel Network Hydrology (Eds. K.J. Beven and M.J. Kirkby). Wiley, Chichester, 128-173.

APPENDIX B. NOTATION

The following symbols are used in this paper:

A_n	cross-sectional area of the flow in zone n, m^2
$A^{(i)}, P^{(i)}$	tridiagonal matrices
$B^{(i)}$	diagonal matrix
C_a	cross-sectional average solute concentration
C_n	cross-sectional average solute concentration in zone n
$C_n(x,t)$	concentration in zone n [at longitudinal spatial co-ordinate x at time t]
$C_{n,i}^k$	value of C_n at grid point $x = x_i$, $t = t_k$

$\underline{c}_n^k$	vector of concentration values C_{nj}^k
D_n	dispersion coefficient in zone n, m^2/s
h_n	depth of zone n
m	mass exchange coefficient between flow and slow zones per unit length per unit time, m^2/s
M	total mass of solute, mg
Q_n	flow rate in zone n, m^3/s
$T(x)$	mean travel time of tracer clouds, s
$T'^2(x)$	temporal variance of tracer clouds, s^2
U_n	average flow velocity in zone n, m/s
U_*	friction velocity (m/s)
w	channel width (m)
β_n	reciprocal of the normalized cross-sectional area of zone n
$\delta(x)$	Dirac delta function
δx	mesh size used in finite difference scheme
δt	time step used in finite difference scheme
Δ'	forward difference operator
Δ''	central difference operator
ΔC	concentration difference between flow and slow zones
$\Gamma_n^{(\nu)}$	ν-th iteration approximation $\underline{c}_n^k$
ε	normalized mass exchange rate coefficient
η_n	normalized cross-sectional area of zone n

APPENDIX C. MASS EXCHANGE COEFFICIENTS

The laboratory experiments were performed to study mass exchange mechanism between flow and slow zones of a pool. Several writers [see for example Westrich, 1976; Valentine and Wood, 1977; Tsai and Holley (1979); Seo, 1990a; Elliott and Brooks, 1997a, 1997b] had undertaken experimental studies to investigate the mass exchange mechanism in the channels. In this study the mass exchange coefficients were measured at various stations along a typical pool of Geometry 1 (pool depth 0.06m) for a variety of flow rates. The longitudinal dimension of the pool was varied in a systematic way, using rectangular blocks of concrete keeping other dimensions same. The mass exchange coefficients were measured at various stations at the interface and at mid pool depth for a variety of flow rates.

To compute mass exchange coefficients between the flow and slow zones in the pool, the dispersion equation (1) of the slow zone was simplified by ignoring advection and dispersion terms. These assumptions were made to simplify the analysis of mass exchange coefficients, and explain why the resulting experimental values of these coefficients for higher pool length were greater than the values used in the numerical simulations. It was further assumed that the tracer solution was directly introduced in the slow zone and the concentration in the flow zone was considered to be zero. Denoting the slow zone concentration by S, the dispersion equation was simplified as

$$A_s \frac{\partial S}{\partial t} = -mS \qquad \text{(C-1)}$$

On integration this gives

$$m = \frac{(\ln S_0 - \ln S) A_s}{} \qquad \text{(C-2)}$$

where A_s is the area and S_0 is the concentration in the slow zone of the pool at $t = 0$. Equation (C-2) indicates that m could have constant values if the concentration decayed exponentially.

A trend of increase in mass exchange coefficients with the increase in flow rate was observed, but a clear relation did not emerge from the results. Moreover, the results showed the effects of change in longitudinal dimension of a pool on mass exchange coefficients. The pool eventually transformed into a dead zone of water by decreasing its length. The mass exchange coefficients decreased by reducing the pool length, which might be due to decreasing advection effects. Table C-1 present the runs average mass exchange coefficient computed at various stations for the Geometry 1-5 shown in Fig. C-1.Table C-2 presents a comparison of non-dimensional mass exchange coefficients with earlier studies.

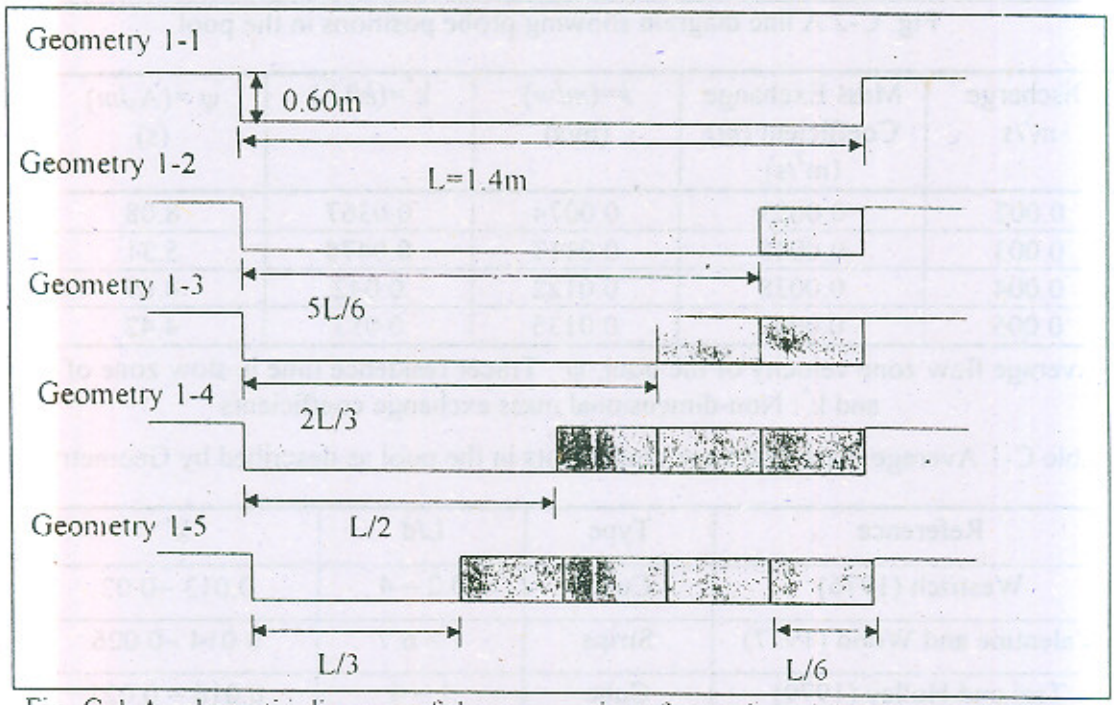

Fig. C-1 A schematic diagram of the geometries of a pool modeled to study the mass exchange coefficients.

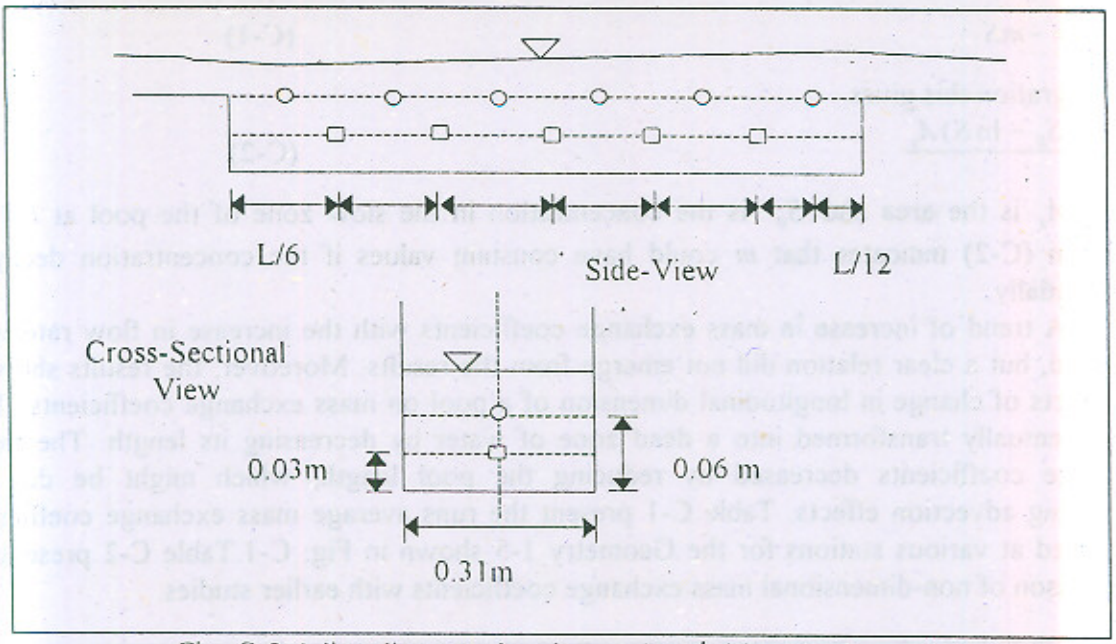

Fig. C-2 A line diagram showing probe positions in the pool.

Discharge m^3/s	Mass Exchange Coefficient (m) (m^2/s)	$k=(m/w)$ (m/s)	$k^*=(k/U^*)$	$\psi=(A_S/m)$ (s)
0.002	0.0023	0.0074	0.0367	8.08
0.003	0.0035	0.0113	0.0478	5.31
0.004	0.0038	0.0122	0.042	4.89
0.005	0.0042	0.0135	0.053	4.42

U^*: Average flow zone velocity of the pool, ψ : Tracer residence time in slow zone of the pool and k^*: Non-dimensional mass exchange coefficients

Table C-1 Average mass exchange coefficients in the pool as described by Geometry 1-5.

Reference	Type	L/d	k^*
Westrich (1976)	Cube	0.2 – 4	0.013 –0.02
Valentine and Wood (1977)	Strips	1 – 6.7	0.014 –0.026
Tsai and Holley (1979)	Cube	1 – 4	0.016 – 0.021
	Strip	9.6	0.027 – 0.061
	Dune	8.0	0.083 – 0.096
Seo (1990)	Pool	10.5 – 11.3	0.044 – 0.071
Present study	Pool	4.66 – 23.3	0.0367 – 0.060

Table C-2 Comparison of non-dimensional mass exchange coefficients with earlier studies.